Original Paper _____ *Forma*, **18**, 133–148, 2003

Deformation of a Neutrally Buoyant Drop of Magnetic Fluid Excited Non-intrusively by an External Magnetic Field

Masanori SATO and Osamu SANO

Department of Applied Physics, Tokyo University of Agriculture and Technology, Koganei, Tokyo 184-8588, Japan
E-mail address: sano@cc.tuat.ac.jp

(Received September 8, 2003; Accepted October 27, 2003)

Keywords: Magnetic Fluid, Neutrally Buoyant, Non-intrusive Excitation, Surface Tension, Maxwell' Stress, Magnetic Susceptibility

Abstract. An experimental study was performed on deformation of a neutrally buoyant drop of a magnetic fluid exposed to a magnetic field. Neutral buoyancy of the drop was realized by placing it in an aqueous solution of lithium bromide whose density was adjusted to the former, and the magnetic field was applied to observe shape change in the absence of contacting solid boundary. When a steady magnetic field was applied, the drop was deformed into an ellipsoid of revolution, whose aspect ratio was determined by the balance of the surface tension and the Maxwell's stress. When the magnetic field was oscillating, eigen modes of oscillation were induced under certain conditions. In other circumstances, shape of the drop changed with frequency two times of the externally applied one. The present method is applicable to estimate surface tension coefficient and magnetic susceptibility of the magnetic fluid.

1. Introduction

Magnetic fluid has attracted much attention among scientists both theoretically and experimentally, because of its peculiar magneto-fluid-mechanical properties as well as wide applications in engineering. Examples of the latter are rotary-shaft seals, levitation devices, sink-float separation processes, impactless printings, optical shutters, energy-conversion schemes, and so forth (see ROSENSWEIG, 1982, 1985, 1987; GOTOH, 1986, for reviews). Quite a number of studies have been made on equilibrium shape and stability of the boundary of magnetic fluid for the past few decades. For instance, instabilities of planar surface and the development into cellular patterns have been investigated both theoretically and experimentally by NEURINGER and ROSENSWEIG (1964), COWLEY and ROSENSWEIG (1967), ZELAZO and MELCHER (1969), ZAITSEV and SHILIOMIS (1969), GALITIS (1977), and others. Equilibrium shapes of the initially spherical or cylindrical magnetic fluid domain under applied magnetic field have also been studied (TARAPOV, 1974; ARKHIPENKO *et al.*, 1978; Gotoh and Yamada, private communication, 1983). Magnetic fluid domain shows elongation in the direction of the magnetic field, which is followed by neck

formation and disruption into smaller droplets for stronger magnetic field.

Theoretical studies often assume magnetic fluid domain which is free from solid boundaries, whereas the presence of the container is inevitable in the experiment. The fluid dynamical behavior, however, depends sensitively on the presence of the solid walls. Indeed instability of the surface of magnetic fluid drop placed on the horizontal plate (MILLER and RESLER, 1975; BRANCHER and ZOUAOUI, 1987), which is subjected to a vertical magnetic field, develops into cone or spike formation above critical magnitude of the magnetic field. Instabilities of a magnetic fluid domain confined between two narrowly spaced parallel plane walls, to which a uniform magnetic field is applied perpendicularly, are observed (ROMANKIW *et al.*, 1975; TSEBERS and MAIOROV, 1980a, b, c), where sequence of transitions of a drop shape from circular disc to elliptic disc ("elliptical" instability), meandering fingers ("serpentine" instability), and disruption into smaller droplets ("overextension" instability) is shown as the magnitude of the field is increased. Similarly a comb-like pattern, in which the mutual invasion of finger-like fluids (i.e. magnetic and non-magnetic fluids) develops into simply connected but highly convoluted region, referred to as labyrinthine structure, has also drawn much attention (ROMANKIW *et al.*, 1975; TSEBERS and MAIOROV, 1980b; ROSENSWEIG *et al.*, 1983; CHUDA and SANO, 1994; PACITTO *et al.*, 2001). All these studies, however, were not entirely free from solid

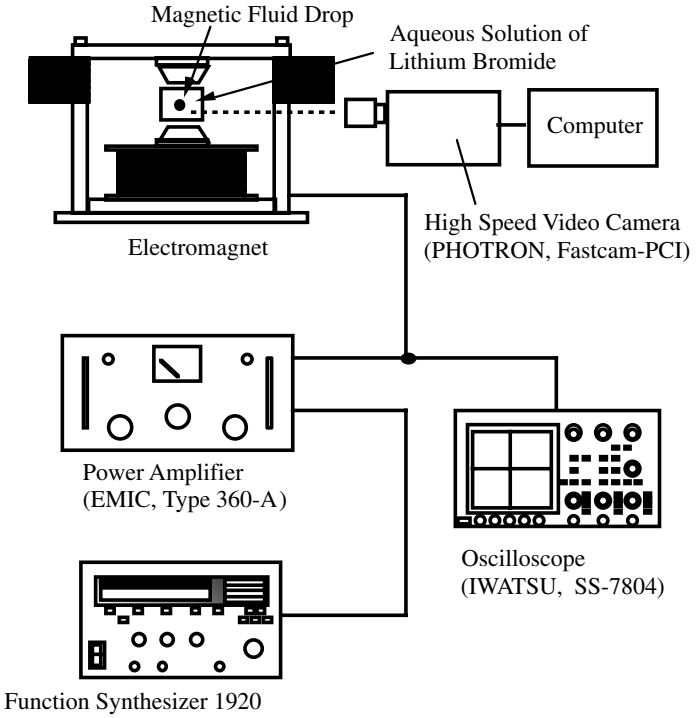

Fig. 1. Experimental apparatus.

boundary which confines the magnetic fluid, so that the properties of a given magnetic fluid and consequently the fluid dynamic behavior also depended on the geometry of the system.

On the other hand, theoretical studies on deformation of a non-magnetic fluid drop, which is not influenced by the presence of a solid boundary nor by the gravity, have been extensively made. In particular, the theory by RAYLEIGH (1879) is well known, which is described in many textbooks (e.g. LANDAU and LIFSHITZ, 1987). Corresponding experimental observation, however, are limited, because of the difficulty of realizing all theoretical requirements. Recently, ARAI *et al.* (1991, 1998) have reported experiments on polyhedral vibration of a spherical drop of non-magnetic fluid. They showed large amplitude axisymmetric mode and tetrahedral mode, each of which is expressed by a single spherical harmonic function (abbreviated as SHF). They also show other regular-polyhedral modes, which are expressed by superposition of several SHFs. In their experiment, however, almost neutrally buoyant drop of orthotoluidine was supported by a thin rod in an aqueous solution of sugar, and was given an oscillation by another thin rod which is connected to a loud speaker, so that two points on the drop were not in free condition. In order to remove the effect of the contacting solid boundary, we performed an experiment on equilibrium shape and dynamic response of a neutrally buoyant magnetic fluid drop, which was *completely free* from solid boundaries and which was excited *non-intrusively* by the magnetic field.

2. Experimental Apparatus

We used paraffin-based magnetic fluid MARPOMAGNA FN-40 (Matsumoto Yushi-Seiyaku Co., Ltd.) as a test liquid, whose density ρ is 1.32 ± 0.05 [g/cm^3] (at 20[°C]),

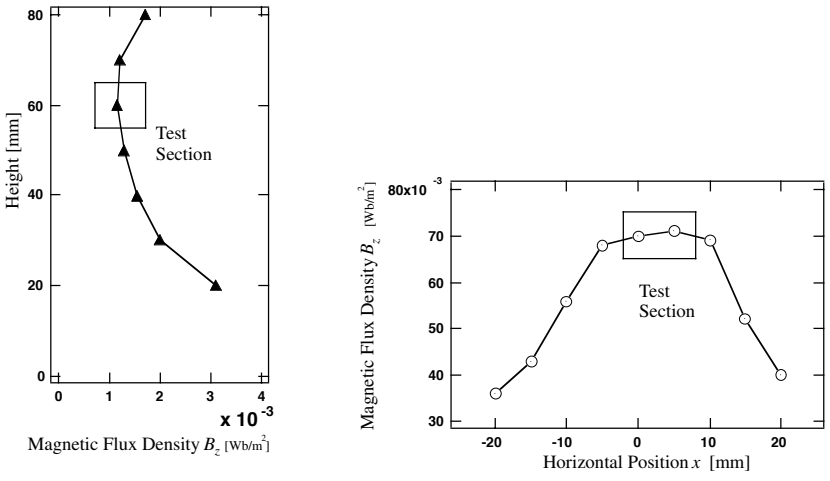

(a) (b)

Fig. 2. Magnetic flux density (a) along the axis and (b) in the mid-plane in the test section. Drop deformation is tested in the region shown by the squares in the above figures.

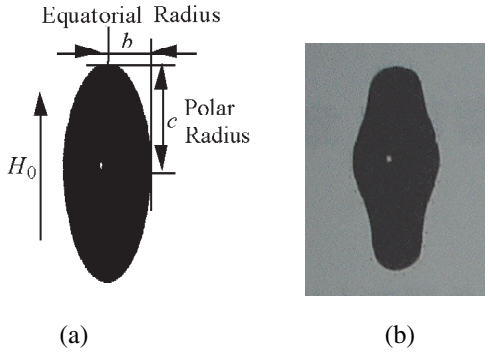

Fig. 3. Deformation of a magnetic fluid drop due to magnetic field.

viscosity η is less than 30 [cP] (at 20[°C]), and magnetization is 400 ± 20 [gauss] for a magnetic field 6000 [Oe]. In order to assure the condition free from solid boundary, we put the material into an aqueous solution of lithium bromide (LiBr). The density of the latter was adjusted so as to keep the drop neutrally buoyant. Shape of the drop in the absence of magnetic field was an almost complete sphere due to the surface tension.

We show our experimental apparatus in Fig. 1. We used a Faraday's electromagnet whose core diameter was 50 [mm] and separation distance of the magnetic poles was 80 [mm]. The magnetic flux density was calibrated by means of the Gauss meter (Yokogawa, Type-3251). We show the magnitude of the field along the axis of the magnet in Fig. 2(a) and that on the mid-plane in Fig. 2(b), which show almost uniform distribution in the region where the drop was placed (shown by the squares in Figs. 2(a) and (b)).

A drop of magnetic fluid of radius R ranging from 1 to 5 [mm] was placed at the center of the magnetic poles, where the magnetic flux density is nearly uniform over the drop. We firstly applied static magnetic field H_0, and the contour shape of the drop was observed by a still-camera. When the static magnetic field was applied, the drop initially spherical was elongated along the field direction, which is well described by an oblate spheroid of revolution (see Subsec. 3.1). Figure 3(a) is an example of the side view of the drop, where the equatorial and polar radii are denoted by b and c, respectively. Secondly we applied a sinusoidally oscillating magnetic field $H = H_0 \sin(2\pi f_{\text{ext}} t)$ to the electromagnet, which was controlled by a function synthesizer (NF ELECTRONIC INSTRUMENTS, Model 1920) and an amplifier (EMIC, Type 360-A). The shape of the drop was observed by means of a high-speed video camera (PHOTRON, Fastcam-PCI). Figure 3(b) is one such example, showing a snapshot of the drop with higher mode and larger deformation. Dependences of the contour shape on the frequency f_{ext} and magnitude H_0 are examined later.

In analyzing the contour image data, we developed a system, in which the contour shape was automatically measured through the following processes:

(i) Successive pictures of the magnetic fluid are taken into a computer.

(ii) Each image data is digitized by setting an appropriate threshold value, so that the drop domain is continuously covered.

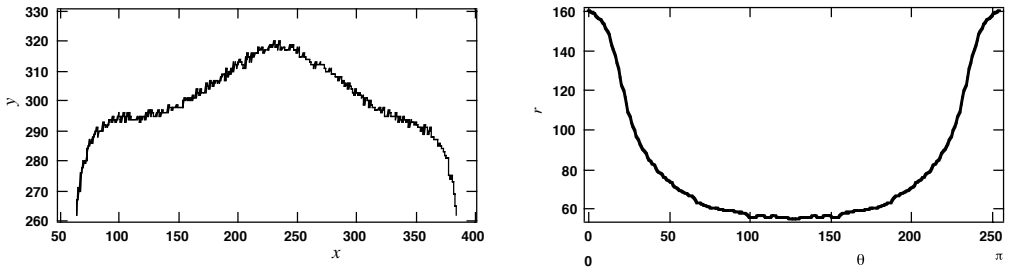

(a) (b)

Fig. 4. Contour shape of the magnetic fluid drop.

(iii) Contour shape is taken out by finding the edge of the drop area (see Fig. 4(a)), whose (x, y) coordinate is stored.

(iv) The (x, y) data is transformed into (r, θ) coordinate, in which the origin is chosen at the center of the contour. Contour shape is described by $r = Rf(\theta)$, where a certain smoothing is made if necessary (see Fig. 4(b)).

(v) Approximate the contour by axisymmetric spherical harmonic functions like

$$r = R[P_0(\cos\theta) + c_2P_2(\cos\theta) + c_4P_4(\cos\theta) + \cdots], \tag{1}$$

where $P_0 = 1$, $P_2 = (3\cos2\theta + 1)/4$, $P_4 = (35\cos4\theta + 20\cos2\theta + 9)/64$, ... are the Legendre polynomials.

(vi) Processes from (ii) to (v) are made for each image data, and time variation of the drop shape is recorded in the case of oscillating magnetic field.

3. Experimental Results

3.1. Equilibrium shape of the drop

Equilibrium shape of the drop is theoretically expected to be determined by the balance of pressure due to surface tension $2\sigma/R^*$ and the magnetic pressure $(1/2)\mu H_0^2$, where σ is the surface tension coefficient, R^* is the mean radius of curvature, μ is the magnetic permeability of the drop, and H_0 is the strength of the externally applied magnetic field. Because of the quadratic dependence on H_0, the drop shape should have fore-and-aft symmetry with respect to the direction of the magnetic field, which was almost ascertained experimentally throughout all tested range of H_0 (see Fig. 3). In order to check the drop shape quantitatively we calculated the volume of the drop by assuming an oblate spheroid of revolution with equatorial radius b and polar radius c (see Fig. 3(a)), which is compared with the initial volume of a sphere of radius R. In all tested cases the agreement is well within an experimental accuracy of about 5%. Figure 5 describes the dependence of polar radius c on the magnetic field, which seems to support quadratic dependence of the elongation of the drop as the magnetic field is increased.

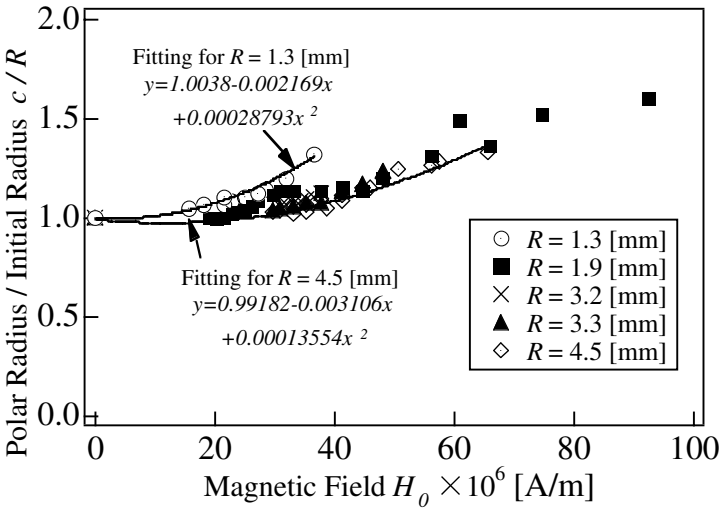

Fig. 5. Dependence of polar radius c on the magnetic field.

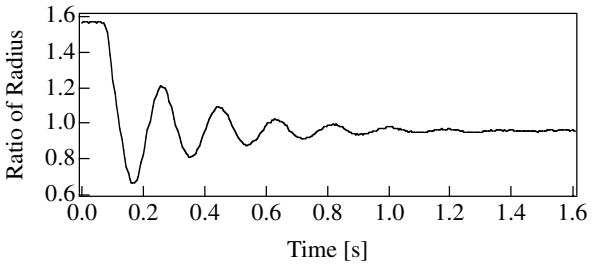

Fig. 6. Damping oscillation of an elongated drop after the magnetic field was switched off (R = 3.6 [mm], H_0 = 2.7 × 10^3 [A/m]).

3.2. Transient behavior of the magnetic drop and the determination of surface tension

When the steady magnetic field was switched off, the elongated magnetic fluid drop showed damping oscillation and approaches to a sphere, which was observed by the high-speed video camera. An example of the time dependence of the ratio of polar to equatorial radii is shown in Fig. 6.

In the case of a spherical drop of inviscid fluid, oscillation of the shape with an infinitely small amplitude is analyzed by RAYLEIGH (1879): the eigen frequency of mode l corresponding to an axisymetric deformation described by $r = R[1 + \varepsilon \exp(-2\pi i f_l t) P_l(\cos\theta)]$ is

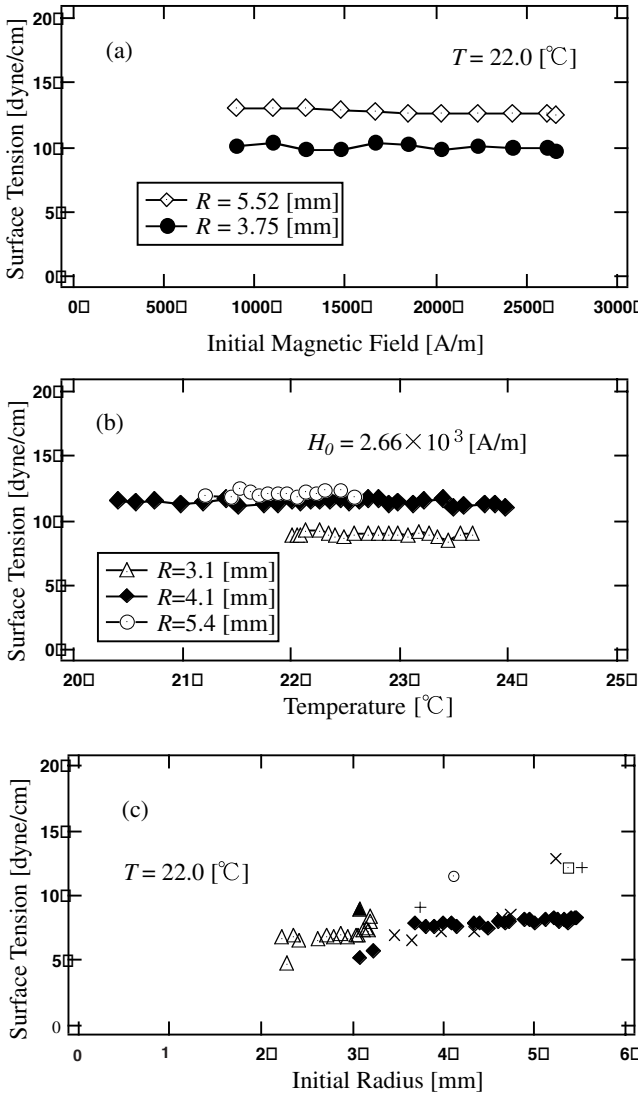

Fig. 7. Dependence of surface tension (a) on the magnetic field, (b) on the temperature and (c) on the initial size of the drop.

$$f_l = \frac{1}{2\pi}\sqrt{\frac{\sigma l(l-1)(l+2)}{\rho R^3}}, \tag{2}$$

where σ is the surface tension coefficient, ρ is the density and R is the mean radius of the drop. For the lowest mode $l = 2$, the frequency is given by

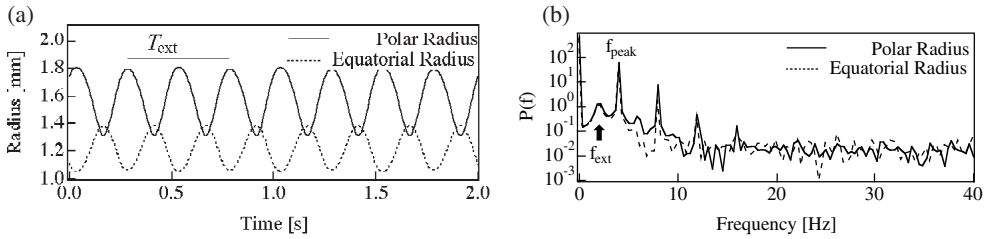

Fig. 8. (a) Time variation of polar and equatorial radii and (b) their power spectra: R = 1.3 [mm], H_0 = 0.81 × 10^3 [A/m], f_{ext} = 2.0 [Hz].

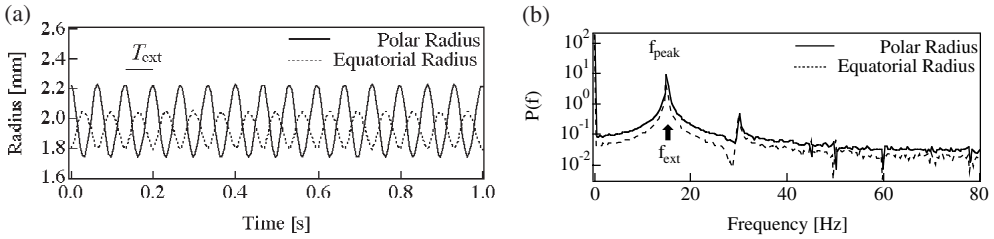

Fig. 9. (a) Time variation of polar and equatorial radii and (b) their power spectra: R = 1.9 [mm], H_0 = 2.64 × 10^3 [A/m], f_{ext} = 15.0 [Hz].

$$f_2 = \frac{1}{2\pi}\sqrt{\frac{8\sigma}{\rho R^3}}, \tag{3}$$

which mainly describes oscillation of our drop in the absence of magnetic field, although both the polar and equatorial radii show damping oscillation due to viscosity. In order to estimate the effect of the viscosity, we assume damping oscillation of the form:

$$c = c_0 \exp(-2\pi\gamma t)\cos\left(2\pi\sqrt{f_2^2 - \gamma^2}\,t\right), \tag{4}$$

where γ is a friction coefficient, f_2 is the frequency in the absence of viscosity and c_0 is the initial polar radius. From successive peak values as shown in Fig. 6 we can estimate γ, whereas successive periods $T = 1/f, f = \sqrt{f_2^2 - \gamma^2}$ are used to determine the eigen frequency f_2. Consequently we can estimate the surface tension σ of the magnetic fluid in aqueous solution of lithium bromide (*ca.* 35%) from Eq. (3).

Figure 7(a) shows the relation of surface tension σ to the magnetic field, whose dependence is rather weak. This result is expected from theoretical point of view, because Maxwell's stress, and hence H_0, μ and μ_0, is relevant only at the initial elongation of the

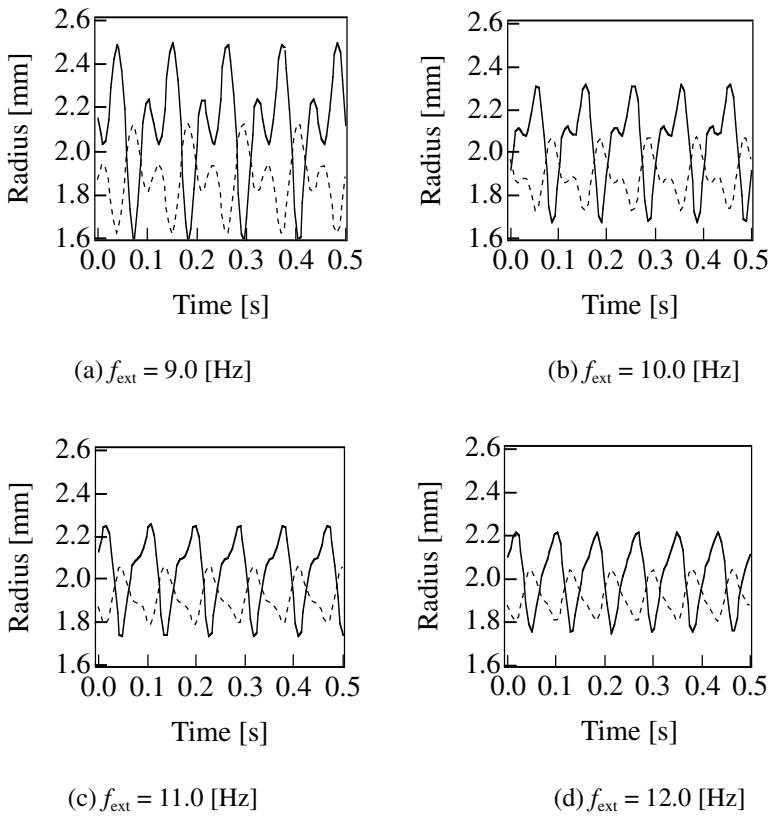

Fig. 10. Time variation of polar and equatorial radii for a drop R = 1.9 [mm].

drop. Figure 7(b) also shows weak dependence of σ on temperature T. But it refers to only a confined range T = 20~24[°C], in which our measurement was performed, so that it does not exclude the possibility of temperature dependence of σ in wide range. On the contrary, considerable dependence of σ on the size of the drop is recognized in Fig. 7(c). Since we focus our attention to the eigen mode f_2, in which effects of magnetic field, temperature and viscous damping have been removed, the cause of the size dependence will be attributed to the deviation from the assumption of infinitesimal deformation in Rayleigh's theory. In fact when the deformation of the drop is larger, the surface area and the effective radius of the drop become larger, so that the estimated value of σ becomes larger. In this context, the limiting value of σ associated with the smallest drop, where surface tension is sufficiently large to keep the latter spherical, will be the most reliable one. Measurement of the drop size, however, becomes poorer for smaller drops. Thus we approximate all the data by least-squares fitting, and extrapolate the relation to R = 0, by which we obtain σ = 6.32 ± 0.27 [dyn/cm] at temperature 22.0[°C].

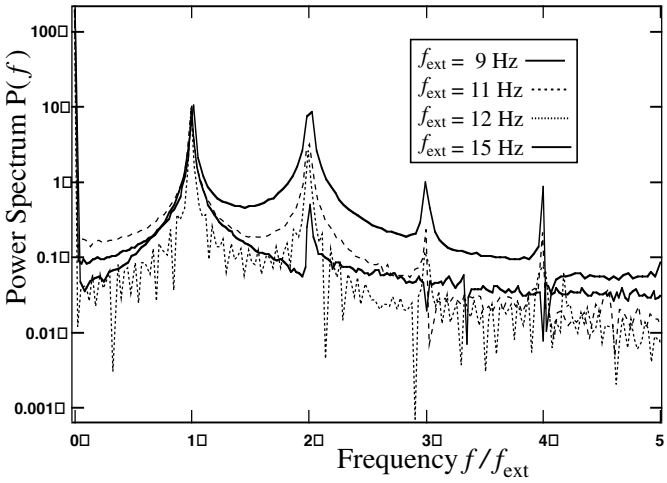

Fig. 11. Spectrum of the time variation of polar radius of a drop R = 1.9 [mm].

3.3. Oscillatory behavior of the magnetic drop under alternating magnetic field

We show the oscillatory behavior of the magnetic fluid drop under externally applied magnetic field $H = H_0 \sin(2\pi f_{ext} t)$. Figures 8(a) and (b) show the time variations and their power spectra, respectively, of the polar radius (solid line) and equatorial radius (broken line) of the drop. The primary oscillation frequency of the drop was two times of the externally applied one (i.e. $f_{peak} = 2f_{ext}$). The deformation was dominated by the applied magnetic field, so that it occurred symmetrically irrespective of the sign of the magnetic field.

On the other hand, Figs. 9(a) and (b) are the time variations and their power spectra, respectively, which shows that a certain eigen mode of oscillation with the same period of the external field (i.e. $f_{peak} = f_{ext} = f_2$) was induced. Between these two typical cases, several mode mixings were observed (see Figs. 10(a)–(d)). We also show their power spectra in Fig. 11. The amplitude of the oscillation with frequency $2f_{ext}$ decreases as the frequency f_{ext} increases (see Figs. 10(a)–(d) and 11), so that the oscillation type changes from forced modes to eigen modes.

In the case of larger drop under larger sinusoidal magnetic field, we had higher mode oscillation of the contour shape. Figure 12 is an example, where a few typical phases within a particular mode are shown. In contrast to ARAI *et al.* (1991, 1998), where both axisymmetric and asymmetric modes were artificially excited, all deformations observed in our experiment were axisymmetric ones. Due to inertia effect, polar radius c/R amounted to as large as 2.7 in the above example but no disruption was observed in the tested range of magnetic field strength.

3.4. Pattern diagram of the oscillation

We show the pattern diagram of oscillation modes in Fig. 13, where the abscissa is the normalized frequency $f^* = f_{ext}/f_2$ and the ordinate is the ratio of magnetic pressure to surface

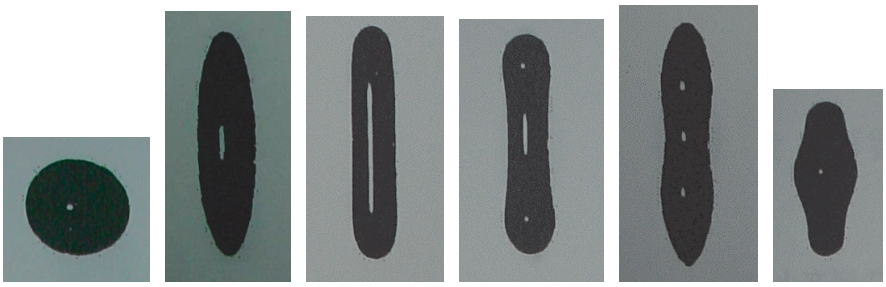

Fig. 12. Snapshots of the large amplitude deformation: $R = 3.99$ [mm], $H_0 = 7.2 \times 10^3$ [A/m], $f_{ext} = 4.0$ [Hz]. (a) $t = 0$, (b) $t = 0.240T$, (c) $t = 0.368T$, (d) $t = 0.496T$, (e) $t = 0.624T$, (f) $t = 0.867T$. T is the period of external field.

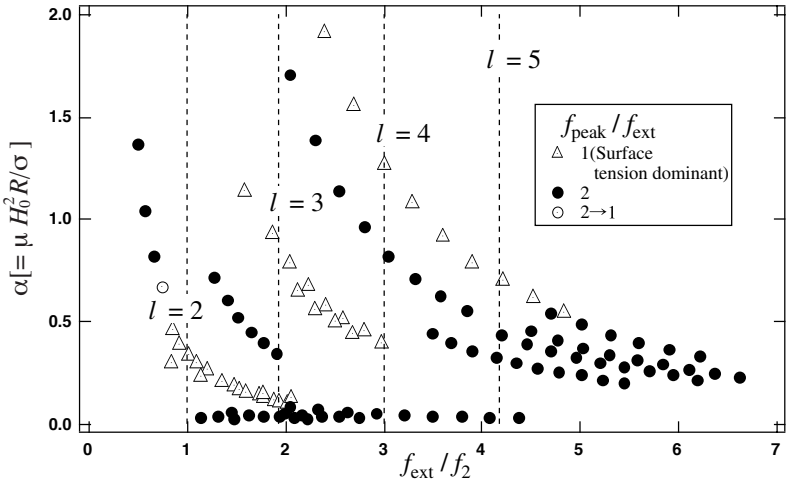

Fig. 13. Pattern diagram of oscillation.

tension $\alpha = \mu H_0^2 R/\sigma$. We see that successive eigen modes (shown by open triangles) were induced with the increase of external oscillation. Vertical lines in Fig. 13 correspond to eigen frequencies normalized by f_2, whose values are 1, $\sqrt{15}/2 \fallingdotseq 1.936$, 3, $\sqrt{70}/2 \fallingdotseq 4.183$, ... for $l = 2, 3, 4, 5, \ldots$, respectively.

4. Discussion

4.1. Equilibrium shape of a magnetic fluid drop with small deformation

The static deformation of a magnetic fluid drop is determined by the balance of

Maxwell's stress with surface tension. The contour shape in the meridian plane is given by SANO (1996) as follows (see also Appendix):

$$\frac{r}{R} = 1 + \frac{\varepsilon}{6}(1 + 3\cos 2\theta) + \frac{19\mu + 26\mu_0}{80(\mu + 2\mu_0)}\varepsilon^2\left\{\cos 4\theta - \frac{4(37\mu + 38\mu_0)}{3(19\mu + 26\mu_0)}\cos 2\theta - \frac{1003\mu + 1332\mu_0}{45(19\mu + 26\mu_0)}\right\} + \mathrm{L}\,, \tag{5}$$

$$= 1 - \frac{4}{45}\varepsilon^2 + \frac{2}{3}\varepsilon\left\{1 - \frac{2(79\mu + 86\mu_0)}{105(\mu + 2\mu_0)}\varepsilon\right\}P_2(\cos\theta) + \frac{4(19\mu + 26\mu_0)}{175(\mu + 2\mu_0)}\varepsilon^2 P_4(\cos\theta) + \mathrm{L}\,, \tag{6}$$

where

$$\varepsilon = \frac{9R\mu_0(\mu - \mu_0)^2}{8\sigma(\mu + 2\mu_0)^2}H_0^2$$

and μ_0 is the magnetic permeability of the ambient fluid. Up to O(ε), the polar radius of the drop is derived from Eq. (5) by putting $\cos\theta = 1$ as follows:

$$\frac{c}{R} = 1 + \frac{3R\mu_0(\mu - \mu_0)^2}{4\sigma(\mu + 2\mu_0)^2}H_0^2, \tag{7}$$

which explains the quadratic increase of c for a given R (see Fig. 5).

4.2. Large deformation of a magnetic fluid drop

Contour shapes of Eq. (5) up to O(ε) are shown in Fig. 14(a), where $\varepsilon = 0$, 0.5 and 1.0. Figure 14(b) is an example of calculation based on the approximation up to O(ε^2), where $\varepsilon = 0.5$ and $\mu/\mu_0 = 1$. Contour shapes, which correspond to different ratios of $P_2(\cos\theta)$ and $P_4(\cos\theta)$, are comparable to Figs. 12(a)–(f), although total volume of the drop is not conserved in the present calculation.

4.3. Measurement of magnetic fluid properties

As has been shown in Subsec. 3.2, we can estimate surface tension coefficient of the magnetic fluid by measuring damping oscillation after the magnetic field is switched off. In addition if we make use of the measured data of c (polar radius of the equilibrium shape of the magnetic drop of radius R) under given magnetic field H_0, we can estimate relative magnetic permeability μ/μ_0, or magnetic susceptibility $\chi = \mu/\mu_0 - 1$ through Eq. (7). Rough estimate of the latter is $(7 \pm 3) \times 10^{-5}$. At this moment the accuracy of our measurement of the equilibrium shape is not sufficient to give more accurate value, which should be improved in future investigation.

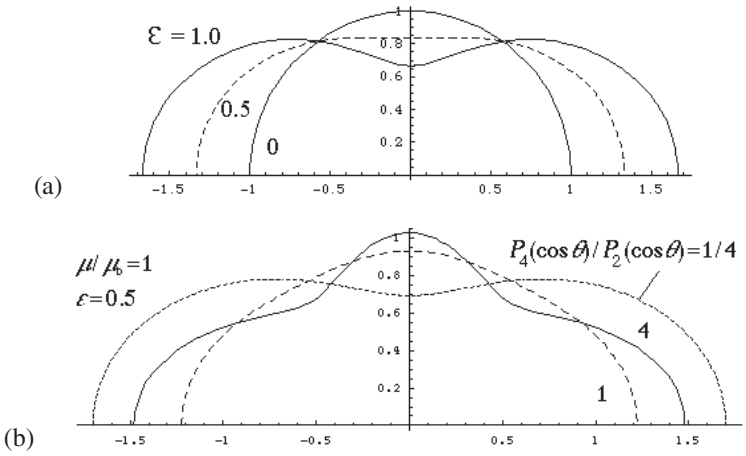

Fig. 14. Contour shapes of an oscillating magnetic fluid drop.

Appendix

Derivation of Eq. (5) is given here. The equilibrium shape of a magnetic fluid drop is determined by the following boundary conditions. Let $\boldsymbol{H}$ and $\boldsymbol{B}$ denote the magnetic field and the magnetic flux density, respectively. Continuities of the tangential components of the former $\boldsymbol{H}_t$ and the normal component of the latter B_n, are required on the boundary:

$$\left\{\boldsymbol{H}_t\right\} = 0, \tag{A1}$$

$$\left\{B_n\right\} = 0, \tag{A2}$$

where $\{Q\} = Q^{\text{out}} - Q^{\text{in}}$ denotes the difference of a quantity Q of outside value from inside one. Balance of Maxwell's stress T_{ij} and surface tension is given by (IMAI, 1989)

$$\left\{\boldsymbol{T}_{\boldsymbol{n}}\right\} \equiv \frac{1}{2}\left(\mu - \mu_0\right)\left(\frac{B_n^2}{\mu\mu_0} + \boldsymbol{H}_t^2\right)\boldsymbol{n} = \sigma\left(\frac{1}{R_1} + \frac{1}{R_2}\right)\boldsymbol{n}, \tag{A3}$$

where μ and μ_0 are the magnetic permeabilities inside and outside of the drop, respectively, R_1 and R_2 are the radii of curvature of the drop, respectively, and $\boldsymbol{n}$ is the outward unit vector normal to the boundary. We assume an axial symmetry as well as fore-and-aft symmetry of the drop, so that the shape of the drop is given by (see Fig. A1)

$$\frac{r}{R} = f(\theta) \equiv 1 + \varepsilon\, c_1 \sin^2\theta + \varepsilon^2 c_2 \sin^4\theta + \mathrm{L}\ .$$

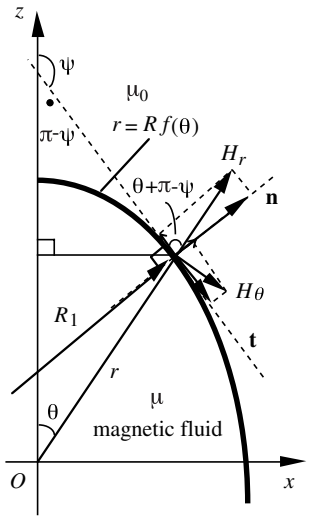

Fig. A1. Definition sketch of the coordinate axes.

Then we have, for example, normal and tangential components of $\boldsymbol{H}$:

$$H_n = \frac{fH_r - f'H_\theta}{\sqrt{f^2 + f'^2}}, \tag{A4}$$

$$H_t = \frac{fH_\theta + f'H_r}{\sqrt{f^2 + f'^2}}, \tag{A5}$$

and

$$\frac{1}{R_1} = \frac{1}{\sqrt{f^2 + f'^2}}\left(1 + \frac{f'^2 - ff''}{f^2 + f'^2}\right), \tag{A6}$$

$$\frac{1}{R_2} = \frac{1}{\sqrt{f^2 + f'^2}}\left(1 - \frac{f'\cos\theta}{f\sin\theta}\right). \tag{A7}$$

Magnetic field potentials inside and outside of the drop ϕ^{in} and ϕ^{out}, respectively, which is exposed to a uniform magnetic field $\boldsymbol{H}_0$ in the z-direction, are, after some calculation,

$$\phi^{\text{in}} = -\left(H_0 - A\right) r P_1(\cos\theta) + \varepsilon\left[A_1 r P_1(\cos\theta) + A_3 r^3 P_3(\cos\theta)\right] + \varepsilon^2\left[a_1 r P_1(\cos\theta) + a_3 r^3 P_3(\cos\theta) + a_5 r^5 P_5(\cos\theta)\right] + \text{L}\ , \tag{A8}$$

$$\phi^{\text{out}} = -\left(H_0 r - \frac{A}{r^2}\right) P_1(\cos\theta) + \varepsilon\left[\frac{B_1}{r^2} P_1(\cos\theta) + \frac{B_3}{r^4} P_3(\cos\theta)\right] + \varepsilon^2\left[\frac{b_1}{r^2} P_1(\cos\theta) + \frac{b_3}{r^4} P_3(\cos\theta) + \frac{b_5}{r^6} P_5(\cos\theta)\right] + \text{L}\ , \tag{A9}$$

where

$$A = \frac{\mu - \mu_0}{\mu + 2\mu_0} H_0, \quad A_1 = \frac{12\mu_0(\mu - \mu_0)}{5(\mu + 2\mu_0)^2} H_0, \quad B_1 = \frac{6(\mu + 4\mu_0)(\mu - \mu_0)}{5(\mu + 2\mu_0)^2} H_0,$$

$$A_3 = 0, \quad B_3 = -\frac{6(\mu - \mu_0)}{5(\mu + 2\mu_0)} H_0, \quad a_1 = b_1 = 0,$$

$$a_3 = \frac{32\mu_0(2\mu^2 + 5\mu\mu_0 - 7\mu_0^2)}{9(\mu + 2\mu_0)^2(3\mu + 4\mu_0)} H_0, \quad b_3 = \frac{4(-41\mu^3 - 81\mu^2\mu_0 + 90\mu\mu_0^2 + 32\mu_0^3)}{15(\mu + 2\mu_0)^2(3\mu + 4\mu_0)} H_0,$$

$$a_5 = \frac{16\mu_0(-\mu^2 - 2\mu\mu_0 + 3\mu_0^2)}{5(\mu + 2\mu_0)^2(5\mu + 6\mu_0)} H_0, \quad b_5 = \frac{8(50\mu^3 + 77\mu^2\mu_0 - 79\mu\mu_0^2 - 48\mu_0^3)}{45(\mu + 2\mu_0)^2(5\mu + 6\mu_0)} H_0,$$

$$c_1 = -1, \quad c_2 = \frac{19\mu + 26\mu_0}{10(\mu + 2\mu_0)}, \ \text{K}\ , \quad \varepsilon = \frac{9R\mu_0(\mu - \mu_0)^2}{8\sigma(\mu + 2\mu_0)^2} H_0^2. \tag{A10}$$

By the constraint that the volume of the drop is conserved, the shape of the magnetic fluid drop is given by

$$\frac{r}{R} = \left(1 - \frac{2}{3}\varepsilon c_1 + \frac{16}{45}\varepsilon^2 c_1^2 - \frac{8}{15}\varepsilon^2 c_2 + \text{L}\ \right)\left[1 + \varepsilon c_1 \sin^2\theta + \varepsilon^2 c_2 \sin^4\theta + \text{L}\ \right], \tag{A11}$$

which leads to Eq. (5). The expression (6) is obtained by rewriting the trigonometric functions by the Legendre's polynomials.

REFERENCES

ARAI, Y., ADACHI, K. and TAKAKI, R. (1991) Spherical harmonic functions for expression of polyhedral vibration of a spherical drop, *Forma*, **6**, 193–204.

ARAI, Y., KASHIWABARA, M. and TAKAKI, R. (1998) Vibrational modes of a spherical drop and spherical harmonic functions, *Forma*, **13**, 31–45.

ARKHIPENKO, V. I., BARKOV, Yu. D. and BASHTOVOI, V. G. (1978) Shape of magnetized fluid in a homogeneous magnetic field, *Magnitnaya Gidrodinamika*, No. 3, 131–134.

BRANCHER, J. P. and ZOUAOUI, D. (1987) Equilibrium of a magnetic liquid drop, *J. Magnetism and Magnetic Materials*, **65**, 311–314.

CHUDA, T. and SANO, O. (1994) Instability of the water-ferrofluid interface and the formation of labyrinthian structure in a Hele-Shaw cell, *Forma*, **9**, 37–50.

COWLEY, M. D. and ROSENSWEIG, R. E. (1967) The interfacial stability of a ferromagnetic fluid, *J. Fluid Mech*., **30**, 671–688.

GALITIS, A. (1977) Formation of the hexagonal pattern on the surface of a ferromagnetic fluid in an applied magnetic field, *J. Fluid Mech*., **82**, 401–413.

GOTOH, K. (1986) Hydrodynamics of magnetic fluids, *Nagare*, **5**, 16–26 (in Japanese).

IMAI, I. (1989) *Denjiki Gaku o Kangaeru* (*Reconstruction of Electricity and Magnetism*) Chap. 6, Science Inc., Tokyo, pp. 157–183 (in Japanese).

LANDAU, L. D. and LIFSHITZ, E. M. (1987) *Fluid Mechanics*, 2nd Ed., Chap. 7, Pergamon, pp. 244–247.

MILLER, C. W. and RESLER, E., Jr. (1975) Magnetic forces and the surface instability in ferromagnetic fluids, *Phys. Fluids*, **18**, 1112–1118.

NEURINGER, J. L. and ROSENSWEIG, R. E. (1964) Ferrohydrodynamics, *Phys. Fluids*, **7**, 1927–1937.

PACITTO, G., FLAMENT, C. and BACRI, J.-C. (2001), Viscous fingering in a magnetic fluid. II. Linear Hele-Shaw flow, *Phys. Fluids*, **13**, 3196–3203.

RAYLEIGH, Lord (1879) *Proc. Roy. Soc. London*, **29**, 71 (through ref. LANDAU and LIFSHITZ, 1987).

ROMANKIW, L. T., SLUSARCZUK, M. G. and THOMPSON, D. A. (1975) Liquid magnetic bubbles, *IEEE Transactions on Magnetics*, **11**, 25–28.

ROSENSWEIG, R. E. (1982) Magnetic fluids, *Sci. Am*., **247**, 136–145.

ROSENSWEIG, R. E. (1985) *Ferrohydrodynamics*, Cambridge Univ. Press, Cambridge.

ROSENSWEIG, R. E. (1987) Magnetic fluids, *Ann. Rev. Fluid Mech*., **19**, 437–463.

ROSENSWEIG, R. E., ZAHN, M. and SHUMOVICH, R. (1983) Labyrinthian instability in magnetic and dielectric fluids, *J. Magnetism and Magnetic Materials*, **39**, 127–132.

SANO, O. (1996) The deformation of the interface of a neutrally buoyant drop of magnetic fluid, *Proc. 19th Int. Cong. Theor. Appl. Mech*., Kyoto, 1996, 811 pp.

TARAPOV, I. E. (1974) Hydrodynamics of magnetizable and polarizable media, *Izvestiya Akademii Nauk SSSR, Mekhanika Zhidkosti i Gaza*, **5**, 141–144.

TSEBERS, A. O. and MAIOROV, M. M. (1980a) Magnetostatic instabilities in plane layers of magnetizable liquids, *Magnitnaya Gidrodinamika*, No. 1, 27–35.

TSEBERS, A. O. and MAIOROV, M. M. (1980b) Comblike instability in thin layers of a magnetic fluid, *Magnitnaya Gidrodinamika*, No. 2, 22–26.

TSEBERS, A. O. and MAIOROV, M. M. (1980c) Structures of interface of a bubble and magnetic fluid in a field, *Magnitnaya Gidrodinamika*, No. 3, 15–20.

ZELAZO, R. E. and MELCHER, J. R. (1969) Dynamics and stability of ferrofluids: Surface interactions, *J. Fluid Mech*., **39**, 1–24.

ZAITSEV, E. M. and SHILIOMIS, M. I. (1969) Nature of the instability of the interface between two liquids in a constant field, *Dokl. Akad. Nauk. SSSR*, **188**, No. 6, 1261–126.